Journal of The Electrochemical Society, **153** (8) B304-B310 (2006)
0013-4651/2006/153(8)/B304/7/$20.00 © The Electrochemical Society

Impedance Characterization of Anodic Barrier Al Oxide Film Beneath Porous Oxide Layer

Rudolf K. Potucek,[a] Richard G. Rateick, Jr.,[b] and Viola I. Birss[a,*,z]

[a]*Department of Chemistry, The University of Calgary, Calgary, Alberta, Canada T2N1N4*
[b]*Honeywell Engines, Systems and Services, South Bend, Indiana 46620, USA*

Electrochemical impedance spectroscopy (EIS) is a common technique used in the assessment of the thickness of anodic oxide films formed on Al and its alloys. However, it is shown here that the resistance (R) values obtained from EIS data are highly dependent on the solution in which the measurements are made, while the capacitance (C) values are independent of the solution conditions and are therefore a much more reliable means of determining oxide film thickness and other properties. We also show that the experimental EIS data for unsealed porous anodic oxides formed on top of a barrier Al oxide film in acidic solutions exhibit only a single time constant, with very little influence seen from the overlying porous oxide layer on the apparent R and C values. The reason for this is demonstrated by utilizing the Laplace equation to calculate the electric field induced in the oxide, which confirms that the EIS response of these films can generally be assumed to reflect the properties and coverage of the underlying barrier oxide film.
 [DOI: 10.1149/1.2208737]

Manuscript submitted June 24, 2005; revised manuscript received February 27, 2006. Available electronically June 13, 2006.

The formation of anodic oxide films is a common means of achieving corrosion protection of Al and its alloys. For example, the formation of porous oxides, with an underlying compact oxide film, is normally achieved in acidic media, while compact films alone are typically deposited in neutral buffer solutions. Porous oxides are generally preferred vs compact films because they can be formed to high thickness, yield excellent abrasion protection, and, after chemical sealing of the pores, provide improved corrosion resistance. Various techniques, such as eddy current measurements,[1,2] ellipsometry,[3,4] interferometry,[5] X-ray photoelectron spectroscopy (XPS),[6] optical scattering,[7] neutron scattering,[8] and transmission electron microscopy (TEM) imaging[9-11] have been used to study the properties of both compact and porous oxide films formed on Al and its alloys. However, these methods are variously limited by being slow, costly, ex situ, or lacking a means of discriminating between the underlying compact (or barrier) and overlying porous oxide layers.

In contrast, electrochemical impedance spectroscopy (EIS) has been established as a simple, nondestructive in situ technique for determining oxide film thickness,[12-14] as well as for studying the sealing[13,15-18] and dissolution[15,19] processes associated with porous anodic oxide film. In prior studies, it was found that the resulting EIS spectra usually contain a single time constant,[9,20-22] typical of a barrier oxide film,[12] or multiple time constants,[15,16] consistent with either the presence of more than one oxide layer or surface roughness effects.[23] While the literature agrees that one or two time constants may be obtained for porous Al oxide films containing unsealed pores, and that three or more time constants can be seen for sealed or corroded oxide layers, the plethora of equivalent circuits used shows the need for a fundamental understanding of the properties of Al oxide films studied using EIS.

As opposed to sophisticated models, such as the point defect model, which aim to elucidate the conduction processes occurring in oxide films, our research was motivated partly by the observation that the resistance (R) and capacitance (C) values obtained from EIS measurements do not change whether or not an overlying unsealed porous oxide film is present on top of a barrier Al oxide film. Thus, the EIS data do not provide a good measure of total oxide film thickness.[12,13] A similar independence of the impedance response on the pore length (film thickness) has been described for porous metal electrodes,[23] but a good explanation for this has not yet been provided. We show here why the common approach of basing an equivalent circuit on the structure/morphology of the oxide, as done by others previously,[18] may lead to an incorrect interpretation of EIS data. We also show that the barrier oxide film thickness, determined from measured C values, as suggested by Hitzig et al.,[13] should generally be regarded as more reliable than thickness determination from the more commonly used R values.

* Electrochemical Society Active Member.
z E-mail: birss@ucalgary.ca

Experimental

Disk samples of pure Al were prepared from Al rod (3/8 in. diam, 99.99%, AlfaAesar) and the exposed faces were lathe-prepared at 1000 rpm using Relton A9 cutting fluid. Samples were washed with distilled water and sonicated in acetone for 10 min before use to ensure no machining residues were retained on the samples. The samples were then mounted in a Teflon sample holder and sealed with black-rubber O-rings with 0.436 cm^2 of the sample surface exposed to solution (Fig. 1). Sample and sample holder were mounted together as the working electrode (WE), exposed face up, in a glass cell also containing a Pt gauze (99.9%, Aldrich) counter electrode (CE) and a Pt wire (99.99%, Aldrich) electrode used for high-frequency EIS measurements.[24] A platinized Pt gauze electrode was used as a reversible hydrogen electrode (RHE) reference electrode (RE) and was mounted in a separate compartment, connected to the WE compartment by means of a Luggin capillary.

Electrochemical experiments were performed using a Solartron 1287 electrochemical interface and a Solartron 1255 frequency response analyzer, and data acquisition was controlled using CorrWare and Zplot software by Scribner Associates. EIS data fitting was performed using Zview software by Scribner Associates, while additional data modeling was performed with custom-written Perl software. Visualization of electric fields was achieved using AVS Express.

Samples were anodized using a 5 min potential hold at potentials ranging from 2 to 14 V vs RHE. Anodization and impedance measurements were performed at 20°C in unstirred pH 7 borate buffer solution (0.025 M $Na_2B_4O_7$;0.5 M HBO_3), pH 7 phosphate buffer (0.05 M KH_2PO_4;0.291 M NaOH), 1 M H_2SO_4, or 0.4 M H_3PO_4, all without deaeration. All solutions were prepared from analytical grade reagents and ultrapure water (ca. 2 MΩ cm) generated using a Corning MegaPure MP-6A distillation apparatus. Impedance measurements were performed after anodic treatment using 10 mV ac excitation at 100 mV vs RHE dc bias and by scanning from 100 kHz to 50 mHz. Unless otherwise specified, EIS measurements were performed in the same solution as was used for sample anodization.

Results and Discussion

Impact of measurement solution on EIS-determined capacitance (C) and resistance (R) values.— R values derived from EIS measurements have been commonly employed as a measure of oxide

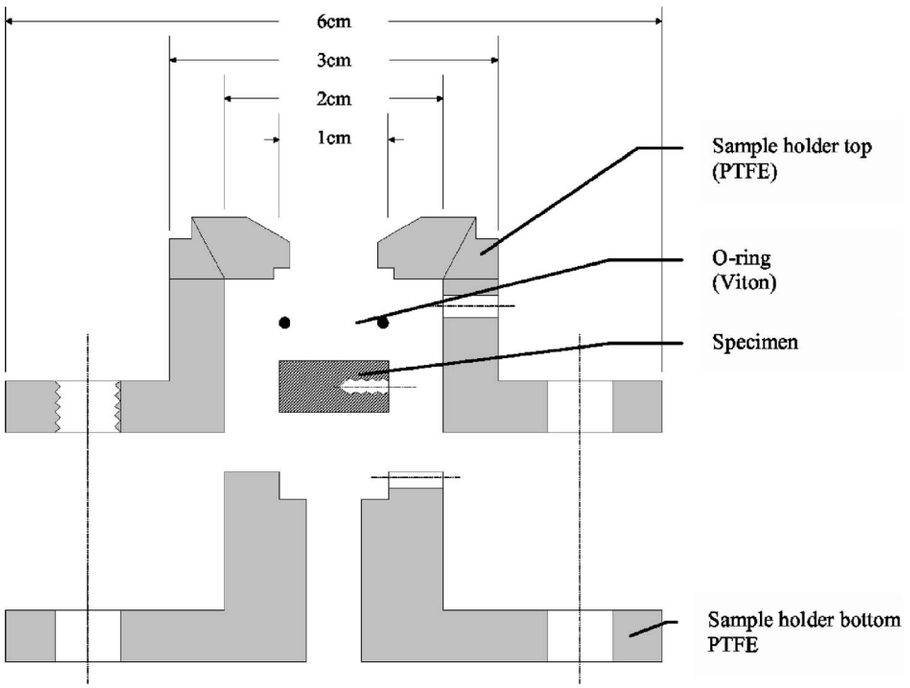

Figure 1. Side view of Teflon sample holder employed to hold disk-shaped Al specimens. The dotted lines indicate locations of screws.

film thickness and of the corrosion resistance of metals,[13,25,26] while impedance-determined[12,13,27] and eddy current-based[1,2] C values have also sometimes been used for oxide film thickness evaluation. Indeed, Eq. 1 shows that both R and $1/C$ should be proportional to the barrier oxide thickness, d. Here, A is the geometric area of the electrode, ρ_{el} is the film resistivity, ε_0 is the permittivity of the vacuum, and ε_r is the permittivity of the oxide film

$$R = \rho_{el}\frac{d}{A} \quad \text{and} \quad C = \varepsilon_0\varepsilon_r\frac{A}{d} \qquad [1]$$

Experimental EIS data, collected at oxide-coated metal electrodes, often show the presence of a constant phase element (CPE, or Q).[28,29] A CPE behaves like a capacitor (C) but has a phase shift of less than 90°, which can also be expressed by an exponent, n, with a value of <1.[13,30,31] Notably, the mathematical simplification of equivalent circuits discussed below applies equally to circuits based on either C or CPE elements, as long as the exponents of all of the CPEs within a particular circuit are equal. Also, the C values resulting from fitting to a CPE are commonly considered comparable for n values greater than approximately 0.8. As the n values in the present work were typically greater than 0.87, capacitors are used in the mathematical representations, even though the discussion applies equally well to CPEs.

In order to confirm the predicted relationships between R, C, and d, oxide films of increasing thickness were formed on pure Al by a series of 5 min applications of a constant anodic potential, incremented in each step by 2 V, followed by the collection of EIS data at 0.1 V in the same solution. For barrier oxide films formed in neutral borate (Fig. 2) and phosphate (not shown) buffer solutions, both R and $1/C$ show the expected linear dependence of film thickness on the anodization potential.[25]

For porous oxide films formed in 0.4 M H_3PO_4 (Fig. 2) and 1 M H_2SO_4 (not shown), a linear correlation of both R and $1/C$ with anodization potential is also seen (Fig. 2). Significantly, the C values are very similar to those obtained for just the barrier oxide films formed at the same potential in neutral solutions, while a large discrepancy is observed between the R values. To explain this, an Al sample was anodized in pH 7 borate buffer at 14 V, conditions under which only a barrier oxide film should form. EIS measurements were then made in this neutral solution, followed by a transfer to 1 M H_2SO_4 for EIS measurements, and then back to neutral borate buffer again. It is seen that the capacitive response (Fig. 3, region 2) remains essentially unchanged, independent of the mea-

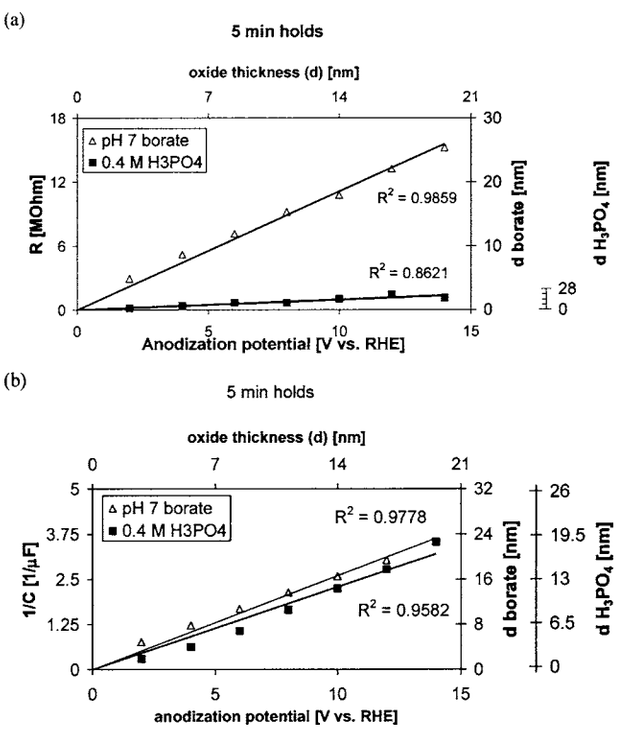

Figure 2. R and $1/C$ values obtained by fitting of EIS data to the equivalent circuit of Fig. 4c. Data were collected at 0.1 V dc bias for pure, emery-paper-polished Al in pH 7 borate buffer and 0.4 M H_3PO_4, with data for each solution collected on a single sample.

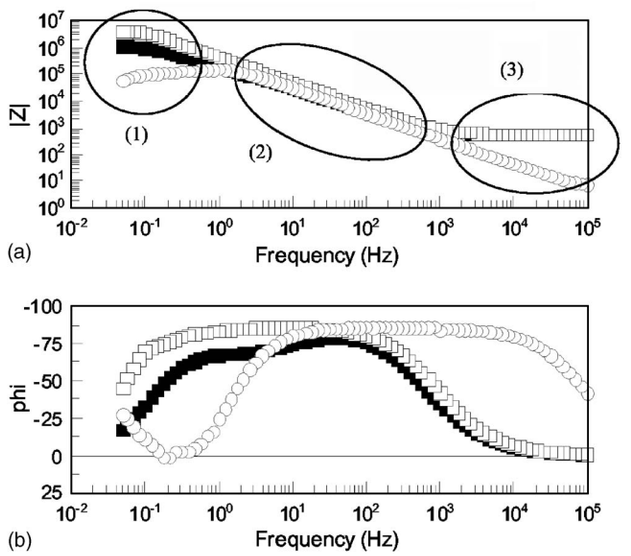

Figure 3. (a) EIS absolute impedance and (b) phase angle spectra of Al sample, anodized for 5 min at 14 V in pH 7 buffer solution, collected at 100 mV dc bias in pH 7 borate (□) before and (○) after exposure to 1 M H_2SO_4. The (1) low, (2) medium, and (3) high-frequency regions are circled in (a).

surement solution, while R (Fig. 3, region 1) is significantly lower when measured in H_2SO_4 vs in the neutral buffer solution.

These results indicate that, for a constant anodizing potential, neither the pH nor the composition of the solution used for anodizing and EIS measurements will significantly affect the measured film capacitance, C, and hence the barrier oxide thickness. However, the R values determined under identical conditions may not be a reliable measure of barrier oxide thickness, especially when EIS data are collected in an aggressive acidic solution. While the resistance values are determined primarily from the low-frequency data, conditions under which measurement noise can be severe and changes in sample properties with time can significantly impact the data, this cannot explain the results shown in Fig. 2. The more likely reason for the dependence of R, but not C, on the pH of the measurement solution lies in the higher number of point defects[32,33] introduced into the oxide film at low pH, thus leading to increased conductivity of the oxide, while leaving the capacitive response essentially unaffected. Therefore, rather than using the R values, the measured CPE values are taken as the indicator of Al oxide film thickness in the present work.

Theoretical derivation of EIS response from porous Al oxide morphology.— While the discussion above demonstrates that C, rather than R, is a better a measure of barrier oxide thickness, we attempt here to provide an explanation as to why the overlying porous Al oxide has no apparent influence on the R or C values determined from EIS measurements.

Simple model: equivalent circuit derived from assumed oxide morphology.— The equivalent circuits presented in the literature are based on the observation that Al oxide is a dielectric material, as indicated by its thickness-dependent capacitive response, and that it has sufficient ionic conductivity to allow the formation of additional oxide under an applied potential. These dual capacitive/conductive (leaky) properties are expressed by the parallel (RC) element.[c] This

[c]For the remainder of this paper, equivalent circuits are presented in the notation introduced by A. Boukamp for his EQUIVCRT software,[34] where a single letter is used to describe a circuit element and consecutive letters denote elements in series or in parallel. Pairs of parentheses change the arrangement from series to parallel and back.

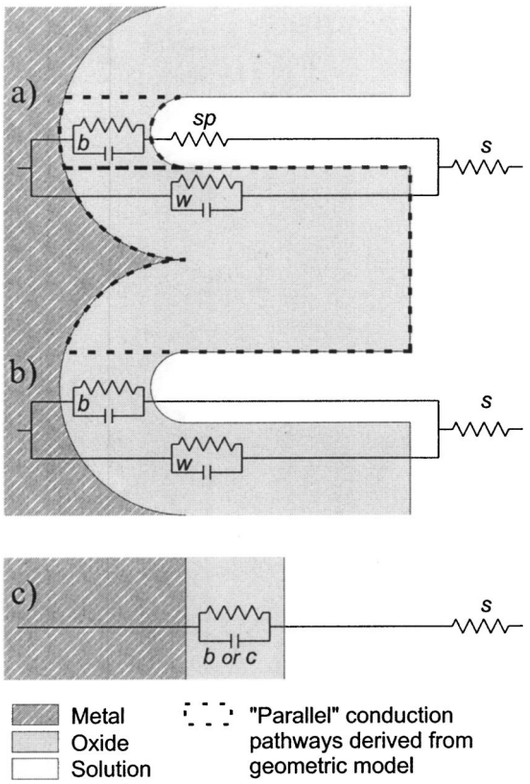

Figure 4. Anodic Al oxide film morphologies showing appropriate equivalent circuit in each case. (a) Porous oxide film and underlying barrier film.[15,16] (b) Same as (a), but circuit simplified by the assumption that $R_{sp} \ll R_s$. (c) Barrier oxide film only,[35] as well as equivalent circuit which applies to composite film EIS response (see text). Subscripts stand for: s-solution, sp-solution in pore, b-barrier, w-pore wall, and c-composite of barrier and wall.

approach works well for barrier oxide films with a homogeneous thickness, leading to the $R_s(R_bC_b)$ circuit (Fig. 4c), where R_s is the solution resistance, R_b is the barrier oxide resistance, and C_b is the barrier oxide capacitance, generally agreeing with experimental observations.[35]

In the presence of an unsealed porous oxide film on top of the barrier oxide (Fig. 4a), we assume that the barrier film exposed to the pore solution, and the barrier film plus overlying porous Al oxide walls, represent two parallel and isolated conduction pathways extending from the metal/metal-oxide (m/o) interface out to the metal-oxide/solution (o/s) interface (Fig. 4a, dashed lines). Thus, the $R_s\{[R_{sp}(R_bC_b)][(R_wC_w)]\}$ circuit (Fig. 4a) is an obvious extension of the barrier oxide equivalent circuit (Fig. 4c). Here, R_{sp} is the solution resistance in the film pores, R_w and C_w are the resistance and capacitance of the porous oxide columns (walls), and R_b and C_b refer to the barrier oxide film.[15,16] Examining the

$$R_s\{[R_{sp}(R_bC_b)][(R_wC_w)]\}$$

circuit (Fig. 4a) suggests that R_{sp} can be ignored when $R_{sp} \ll R_s$, thus simplifying the circuit to $R_s\{[(R_bC_b)][(R_wC_w)]\}$ (Fig. 4b). Using Kirchhoff's rules, this simplified circuit can be further reduced to $R_s(R_cC_c)$(Fig. 4c), with the composite parameters, R_c and C_c, defined by Eq. 2

$$\frac{1}{R_c} = \frac{1}{R_b} + \frac{1}{R_w} \quad \text{or } R_c = \frac{R_bR_w}{R_b + R_w} \quad \text{and } C_c = C_b + C_w \qquad [2]$$

Following Eq. 2, it is apparent that the composite R_c and C_c values should contain a contribution from both the barrier oxide and

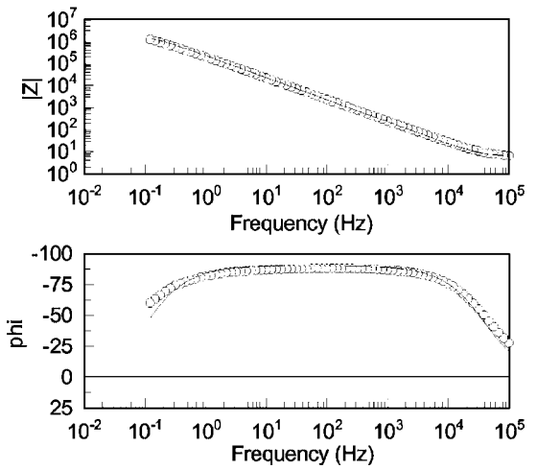

Figure 5. Bode plot of EIS data collected at 0.1 V in 1 M H_2SO_4 at pure Al, anodized in 1 M H_2SO_4 at 14 V for 5 min: (○) Experimental data. (–) Line fitting the data using simple equivalent circuit shown in Fig. 4.

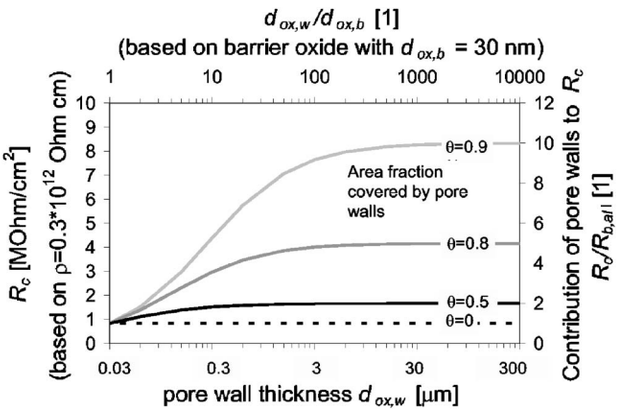

Figure 6. Influence of Al oxide pore wall thickness (=film thickness), $d_{ox,w}$, on R_c values, obtained assuming parallel conduction pathways (Fig. 4b) and a range of porous oxide film coverages (0–90%) of the Al surface.

the pore walls, and should display a dependence on the fraction of the surface, θ, which is covered by the porous oxide film walls

$$\frac{1}{R_c} = \frac{(1-\theta)}{R_{b,\text{all}}} + \frac{\theta}{R_{w,\text{all}}} \quad \text{and} \quad C_c = (1-\theta)C_{b,\text{all}} + \theta C_{w,\text{all}} \quad [3]$$

where $R_{b,\text{all}}$ and $C_{b,\text{all}}$ are the R and C values for a barrier film where θ = 0, and $R_{w,\text{all}}$ and $C_{w,\text{all}}$ are the values for a porous film when θ = 1.

The expressions for R_c and C_c, given by Eq. 3, explain the single time constant (Fig. 5) observed experimentally for Al anodized in H_2SO_4 under conditions known to form porous oxide films on top of the compact oxide layer.[17,25,36-47] Equation 3 also suggests that the individual contribution of the porous film (the pore walls) and of the underlying barrier oxide cannot be extracted from the experimental R_c and C_c values without knowledge of θ. Thus, the experimental EIS data would simply suggest the presence of a barrier oxide film of significantly greater thickness and/or resistivity than is actually the case.

It is instructive, however, to examine how the thickness and coverage of a porous Al oxide film should influence the measured R_c and C_c values, using this simple approach. Assuming a typical anodizing ratio of 1.4 nm/V,[25] an anodizing voltage (sulfuric acid) of 20 V,[25,40,42] and an Al oxide resistivity of 3×10^{11} Ω cm, a barrier oxide thickness of 28 nm and a corresponding $R_{b,\text{all}}$ of 0.84 MΩ/cm^2 are obtained. Varying the thickness of the porous oxide pathway (Fig. 4) from 28 nm to 280 µm yields R_w values ranging from 0.84 MΩ/cm^2 to 8.4 GΩ/cm^2. Using Eq. 3, Fig. 6 shows a plot[d] of R_c as a function of θ. From the plot (Fig. 6), it is apparent that for all values of θ, any further growth of porous oxide film beyond a certain thickness will no longer influence R_c. Based on typical Al oxide pore dimensions reported in the literature,[25] θ after anodization in H_2SO_4 or H_3PO_4 should be >0.90. Thus, the R_c and C_c values, determined from EIS measurements, should yield significantly higher apparent barrier oxide thicknesses for (porous + barrier) films formed in acidic vs neutral solutions, and we should also observe an increase in apparent oxide thickness with formation time in acidic solutions. However, the experimental data do not show either of these effects. As shown below, this is not due to an improper choice of equivalent circuit or incorrect assumptions regarding the conducting pathways of the porous and barrier oxide components as being parallel or in series, but is rather an inherent problem of directly converting oxide geometry to equivalent circuit parameters.

Improved model: determining R_c and C_c from rigorous electric field calculations.— One possible explanation for the minor influence of the porous oxide layer on the impedance response is that independent parallel pathways through the film (barrier film and pores vs walls of porous oxide), as generally postulated in the derivation of equivalent circuits from oxide geometry, cannot legitimately be assumed, considering the relative dimensions of the Al oxide components. For example, the use of parallel plate capacitors is only appropriate if the plate size is significantly larger than the plate separation and if the inhomogeneity in the electric field at the plate edges can be ignored. Considering that the typical pore radius in an Al oxide film is ca. 0.4 nm/V, the cell radius is ca. 1.2 nm/V, and the growth rate is ca. 3–6 nm/s,[25] it is apparent that even at an anodization potential of 20 V, the thickness of the porous oxide film will exceed the width of a pore wall in ca. 24 s, i.e., in a time period significantly shorter than the ca. 1800 s commonly used in commercial anodizing or the 90–300 s used in our experiments. Further, the assumption of independent parallel conduction pathways should be questioned, as the two conduction pathways (Fig. 4a) are in intimate contact, an observation that has led other researchers to use the transmission line model for porous electrodes.[48-50]

To overcome the described failings of deriving equivalent circuits from oxide geometry, we instead propose a more general approach that can be used equally well for data fitting using equivalent circuits and for chemical models, such as the point defect model.[32,33] Based on the single time constant observed, the oxide film is modeled as an (*RC*) element. However, instead of deriving *R* and *C* by simplifying an equivalent circuit, we assume that both the barrier and porous oxide films (Fig. 4) have identical properties and derive the *R* and *C* values from electric field calculations based on the oxide geometry. Thus, it is necessary to determine the electric field throughout the Al oxide film, normally by solving the Poisson equation. However, solving this equation in more than two dimensions is very computationally intensive. Therefore, a simplified set of solutions was calculated by solving the Laplace equation[51] using a finite element approach, similar to that described by Fleig and Maier.[23,52] While this approach ignores the presence of the space-charge region in the oxide, and thus strictly only applies to a completely nonconductive dielectric material, the amount of current passing through the Al oxide is very small, so that neglecting the space charge throughout the oxide will not significantly affect the result of the calculations. Also, the Laplace equation scales well to three dimensions, suggesting that this approach could be used for data fitting.

[d]Using the idealized model presented here, there is no difference in the findings from either R_c or $1/C_c$, as both depend linearly on the oxide thickness (Eq. 1).[13] Thus, only R_c data are presented.

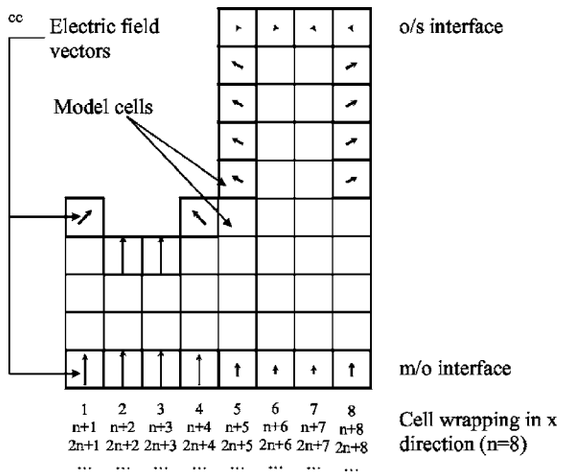

Figure 7. 2D grid representation of porous Al oxide film for the purpose of solving the Laplace equation for the electric field. The grid is wrapped in the *x*-direction to simulate an infinitely repeating surface.

For the numerical calculations in the present work, we chose a simplified 2D grid representation of the oxide geometry (Fig. 7), as it is conceptually straightforward to extend the 2D approach to 3D and as it can be run on a fast PC without major optimization. The grid was wrapped in the x-direction, effectively creating an infinite surface and avoiding edge effects. The electrical potential at the m/o interface was set to 0 V and the potential at the o/s interface to an arbitrary value of 9 V, consistent with many of our anodization experiments. While fixing the latter interface potential at a constant value at all points ignores the contribution of the pore solution resistance, this approximation appears reasonable, considering that the resistivity of the Al oxide pore walls (ca. 10^{11}–10^{14} Ω cm) will significantly exceed the resistivity of the pore solution (ca. 10–100 Ω cm). Using the electric potential, ϕ_{el}, and electric field, **E**, resulting from solving the Laplace equation, it is then possible to derive the *R* and *C* values for an individual grid cell by rearranging Eq. 4 for *d* and substituting into Eq. 1

$$|\mathbf{E}| = \phi_{el}/d \qquad [4]$$

This yields Eq. 5

$$R = \rho_{el}\frac{\phi_{el}}{A(\mathbf{e}_n\mathbf{E})} \quad \text{and} \quad C = \varepsilon_0\varepsilon_r\frac{A}{\phi_{el}}(\mathbf{e}_n\mathbf{E}) \qquad [5]$$

Here, $\mathbf{e}_n$ is the unit vector surfacing a direction of interest. To determine the *R* and *C* values, it is necessary to integrate along an isopotential line.[52] For convenience, we have chosen the isopotential line at the m/o interface, because the electric field vector is perpendicular to the surface at all grid points and the $\mathbf{e}_n\mathbf{E}$ term simplifies to $|\mathbf{E}|$, yielding

$$R = \rho_{el}\frac{\phi_{el}}{A|\mathbf{E}|} \quad \text{and} \quad C = \varepsilon_0\varepsilon_r\frac{A}{\phi_{el}}|\mathbf{E}| \qquad [6]$$

Finally, integration of the resulting *R* and *C* values along the selected surface yields the total R_c and C_c values for the oxide geometry studied, i.e., the barrier oxide plus its overlying porous oxide film.[52]

Examining the distribution of the electric field (Fig. 8) shows that the majority of the potential drop (densely spaced isopotential lines) occurs over a distance comparable to the thickness of the barrier oxide at the pore base (Fig. 4a, dashed line at pore base), while the pore walls far away from the m/o interface are essentially nonconductive. Figure 8 also implies that the pore walls near the base of the pore exhibit a reactivity similar to that of the exposed barrier oxide. This explains why coverage of most of the Al surface by a porous oxide film does not have as significant an effect on the total measured resistance as predicted (Fig. 6), using equivalent circuits such as those shown in Fig. 4a.

In order to compare the experimentally determined R_c values with those obtained using the Laplace equation, several porous film geometries were examined, with $0 < \theta < 0.9$ and $1 < d_{ox,w}/d_{ox,b} < 100$, where $d_{ox,b}$ is the oxide thickness corresponding to R_b and $d_{ox,w}$ is the oxide thickness corresponding to R_w. Figure 9 reveals that only a small increase in resistance should be observed as porous films are formed, even for θ values as large as 0.9. Consistent with experiments, and according to the solution of the Laplace equation, the point at which any further increase in porous film thickness will no longer influence R_c is predicted by this model to be about 0.1 μm (Fig. 9), as opposed to about 60 μm, predicted by the simple equivalent circuit model (Fig. 4c and 6). Assuming an oxide growth rate of 3–6 nm/s,[25] this thickness should be reached in under 35 s, a time much shorter than that employed in most anodization experiments.

The negligible influence of the porous oxide on the *R* and *C* values predicted using these more rigorous electric field calculations are now fully consistent with the experimental observations. Overall, these calculations suggest that unsealed porous oxide overlayers

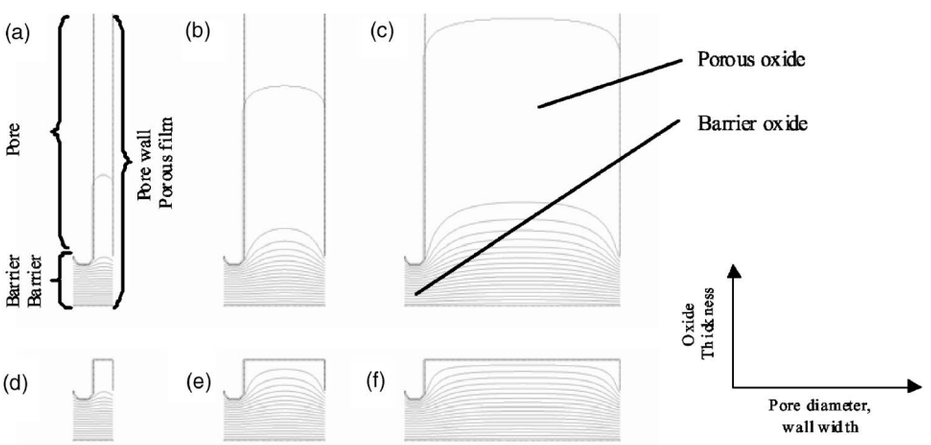

Figure 8. Isopotential lines in cross section of porous Al oxide film, deposited on a compact oxide film, determined by solving the Laplace equation for various 2D oxide layer geometries. The respective geometries correspond to: (a, d) θ = 0.5, (b, e) θ = 0.8, and (c, f) θ = 0.9. Two different pore wall thicknesses [a–c (thicker) vs d–f (thinner)] are shown to demonstrate that the electric potential distribution within the oxide, and thus the calculated *R* and *C* values are only marginally affected by the pore wall thickness.

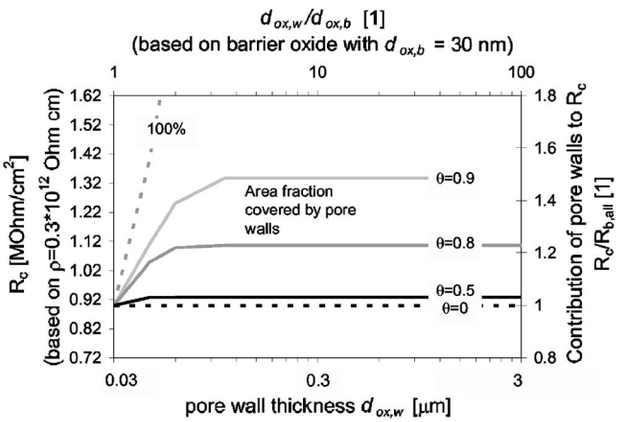

Figure 9. Influence of the relative pore wall thickness on the R_c values for a porous oxide layer. R_c and C_c were determined by solving the Laplace equation for the electric field and calculating R and C at the metal–oxide interface.

can generally not be detected or characterized using EIS. However, EIS (particularly the capacitance values) remains a very good method of characterizing barrier oxide films formed anodically on Al electrodes, even in the presence of an overlying porous oxide film of widely varying thickness.

In addition to explaining the lack of any significant influence of an overlying porous Al oxide film on the observed EIS response, the approach presented here shows promise for modeling the EIS response of porous oxides when the pore diameter changes significantly during an experiment or for the detailed modeling of pore growth. Also, the determination of R_c by solving the Laplace equation is equally possible when using more detailed models, such as the point defect model.[32,33] However, the exact geometry of the porous oxide allows for a limited number of degrees of freedom, such that the use of this model for fitting EIS data will only be possible with well-defined geometries.

EIS determination of other physical properties of barrier Al oxide films.— While independent measurements of Al oxide thickness were not performed in the present work, the data shown in Fig. 2 indicate that a linear correlation between barrier oxide thickness and applied potential can be assumed for films formed in either neutral or acidic solutions, in agreement with past literature.[12,25] By using an anodizing ratio of 1.4 nm/V from the literature[16,25] and the geometric area of the exposed Al surfaces, it is possible to estimate the barrier oxide resistivity, ρ_{el}, and dielectric constant, ε_r, using Eq. 1. The resulting ε_r values range from 13 to 31 (Table I), which is consistent with reported values for hydrated oxide films, e.g., for Zr.[53] However, these values are noticeably higher than the ε_r = 4.5–8.4, reported for dry Al oxide.[54] This suggests that anodically formed oxide films, when examined in situ, are likely highly hydrated.

Table I. Dielectric constant and resistivity of Al oxide barrier film, determined from oxide *C* and *R* values obtained using EIS (Fig. 2), and using calculated oxide film thickness (see text).

Anodizing solution/potential		ε_r	$\rho_{el} \times 10^{12}$ Ω cm
pH 7 borate		16.8 ± 0.8	2.6 ± 1
pH 7 phosphate		31.1 ± 3.9	2.1 ± 0.8
1 M H_2SO_4	(all)	28 ± 18	0.8 ± 1.2
	(>8 V)	13.41 ± 2.1	2.2 (single point)
0.4 M H_3PO_4	(all)	27 ± 11	0.2 ± 0.1
	(>8 V)	18.5 ± 2.1	0.3 ± 0.1

The ρ_{el} values determined from our data, 2×10^{11} to 3×10^{12} Ω cm, are within the range of $\rho_{el} = 10^{11}$–10^{14} Ω cm reported in the literature for dry and hydrated Al oxide.[54,55] Because our measured resistivity values lie at the lower end of this range, this suggests that barrier Al oxide films formed anodically in aqueous solutions are partially hydrated and thus possibly more conductive than dry Al oxide films evaluated by techniques such as eddy current measurements.

Conclusion

The primary focus of this work has been on understanding and improving the interpretation of impedance (EIS) data collected in aqueous solutions at oxide-coated metals such as Al and its alloys. Here, both barrier and porous oxide films were formed on pure Al by stepping to anodization potentials from 2 to 14 V, typically in 2 V increments, and then holding at this value, typically for 5 min, prior to stepping back to 0.1 V, at which the EIS data were normally collected. To form barrier oxide films only, neutral borate or phosphate buffer solutions were used at room temperature, while porous films, with an underlying barrier film, were formed in sulfuric or phosphoric acid media. The porous oxide films were not sealed in this research, being examined immediately after anodic formation, and their thicknesses were estimated to be in the range of 1.5–10.5 μm.

An important finding from this work is that the *R* values obtained from EIS data are highly dependent on the solution in which the measurements are made, while the *C* values are independent of the solution conditions. We speculate that this may be due to the presence of a higher number of point defects[32] in the film in acidic media than in the neutral buffer solutions and a resulting increase in film conductivity, while the oxide thickness remains unchanged. Therefore, the *C* values are shown to be a much more reliable means of determining the Al oxide film thickness, under our experimental conditions.

We have also demonstrated that the experimental EIS data for unsealed porous anodic oxides formed on Al in sulfuric and phosphoric acid solutions exhibit only a single time constant, as expected for barrier oxide films, with very little influence seen of the porous oxide layer on the apparent *R* and *C* values. By utilizing the Laplace equation, we have calculated the electric field induced in the oxide and shown that the straightforward conversion of the geometrical representation of a porous oxide to an equivalent circuit containing parallel (*RC*) components may not sufficiently take into account all of the conductive pathways present within a porous oxide film. In fact, calculation of the electric field across the oxide film leads to *R* and *C* values more consistent with experimental impedance observations, explaining both the single time constant sometimes observed for unsealed porous oxides and the low impact of porous oxide on the EIS response. While electric field calculations cannot be considered as a convenient approach for interpreting EIS data at this point, our electric field modeling shows that the presence of an unsealed porous oxide has almost no impact on the thickness of the barrier oxide determined by EIS, validating EIS as a technique for studying barrier oxide films on Al. In particular, our work shows that the EIS response of unsealed porous oxides, formed on top of the barrier oxide, can generally be assumed to reflect the properties of the underlying barrier oxide film and is thus a suitable technique for studying barrier oxide films, even in the presence of overlying porous oxide layers.

Acknowledgments

We gratefully acknowledge Honeywell, Incorporated, for the financial support of this research. We also thank Dr. E. Donovan, University of Calgary (Department of Physics), for valuable discussions regarding the application of the Laplace equation.

University of Calgary assisted in meeting the publication costs of this article.

References

1. A. Ott, *Aluminium*, **52**, 491 (1976).
2. S. Olbrantz and J. Rasmussen, in *Proceedings of the AESF Annual Technical Conference*, June 21–24, 1999, Cincinnati, OH (1999).
3. J. De Laet, J. Scheers, H. Terryn, and J. Vereecken, *Electrochim. Acta*, **38**, 2103 (1993).
4. T. Schram, J. De Laet, and H. Terryn, *J. Electrochem. Soc.*, **145**, 2733 (1998).
5. K. Habib, *Corros. Sci.*, **43**, 449 (2001).
6. B. Strohmeier, *Surf. Interface Anal.*, **15**, 51 (1990).
7. W. Kessler and R. W. Kessler, in *International Symposium on Aluminium Surface Science and Technology*, H. Terryn and G. Verhoeven, Editors, p. 38, "Elzenveld," Antwerp, Belgium (1997).
8. Z. Tun, J. Noel, and D. Shoesmith, *Physica B*, **241–243**, 1107 (1998).
9. S. Thomas, Ph.D. Thesis, The University of Calgary, Calgary, Alberta, Canada (1994).
10. S. Thomas, V. Birss, and D. Tessier, *Microsc. Res. Tech.*, **31**, 285 (1995).
11. V. I. Birss, S. C. Thomas, and A. J. Zhang, *Electrochim. Acta*, **40**, 1551 (1995).
12. S. Gudic, J. Radosevic, and M. Kliskic, *J. Appl. Electrochem.*, **26**, 1027 (1996).
13. J. Hitzig, K. Juttner, W. Lorenz, and W. Paatsch, *Corros. Sci.*, **24**, 945 (1984).
14. S. Byeon and Y. Tzeng, *J. Electrochem. Soc.*, **135**, 2452 (1988).
15. F. Mansfeld and M. W. Kendig, *J. Electrochem. Soc.*, **135**, 828 (1988).
16. T. Hoar and G. Wood, *Electrochim. Acta*, **7**, 333 (1962).
17. J. Gonzales, V. Lopez, E. Otero, and A. Bautista, *J. Electrochem. Soc.*, **147**, 984 (2000).
18. J. Gonzales, V. Lopez, A. Bautista, E. Otero, and X. Novoa, *J. Appl. Electrochem.*, **29**, 229 (1999).
19. J. Hitzig, K. Juttner, W. Lorenz, and W. Paatsch, *J. Electrochem. Soc.*, **133**, 887 (1986).
20. S. C. Thomas and V. I. Birss, *J. Electrochem. Soc.*, **144**, 1353 (1997).
21. R. Potucek, Ph.D. Thesis, The University of Calgary, Calgary, Alberta, Canada (2004).
22. F. Debuyck, L. Lemaitre, M. Moore, A. van Petegheim, E. Wettinck, and L. Weyten, *Surf. Coat. Technol.*, **34**, 311 (1988).
23. J. Fleig and J. Maier, *Solid State Ionics*, **94**, 199 (1997).
24. F. Mansfeld, S. Lin, Y. C. Chen, and H. Shih, *J. Electrochem. Soc.*, **135**, 906 (1988).
25. J. Diggle, T. Downie, and C. Goulding, *Chem. Rev. (Washington, D.C.)*, **69**, 365 (1969).
26. T. Burleigh and A. Smith, *J. Electrochem. Soc.*, **138**, L34 (1991).
27. M. A. Hill, D. P. Butt, and R. S. Lillard, *J. Electrochem. Soc.*, **145**, 2799 (1998).
28. J. Macdonald, *Solid State Ionics*, **13**, 147 (1984).
29. A. Jonscher, *Nature (London)*, **250**, 191 (1974).
30. R. Hurt and J. Macdonald, *Solid State Ionics*, **20**, 111 (1986).
31. G. Brug, A. van den Eeden, M. Sluyters-Rehbach, and J. Sluyters, *J. Electroanal. Chem. Interfacial Electrochem.*, **176**, 275 (1984).
32. C. Chao, L. Lin, and D. D. Macdonald, *J. Electrochem. Soc.*, **128**, 1187 (1981).
33. L. Zhang, D. Macdonald, E. Sikora, and J. Sikora, *J. Electrochem. Soc.*, **145**, 898 (1998).
34. B. Boukamp, *Solid State Ionics*, **20**, 31 (1986).
35. J. Randles, *Discuss. Faraday Soc.*, **1**, 11 (1946).
36. J. Macdonald, *Solid State Ionics*, **13**, 147 (1984).
37. J. Macdonald, *J. Appl. Phys.*, **62**, R51 (1987).
38. Y. Fukuda and T. Fukushima, *Electrochim. Acta*, **28**, 47 (1983).
39. Y. Fukuda, T. Fukushima, and M. Nagayama, *Transactions of National Research Institute for Metals*, **32**, 29 (1990).
40. M. Lerner, in *Aluminum Surface Treatment Technology*, R. S. Alwitt and G. E. Thompson, Editors, PV 86–11, p. 47, The Electrochemical Society Proceedings Series, Penington, NJ (1986).
41. O. Jessensky, F. Mueller, and U. Goesele, *J. Electrochem. Soc.*, **145**, 3735 (1998).
42. M. B. Spoelstra, D. H. van der Wejde, A. J. Bosch, and J. H. W. de Wit, in *International Symposium on Aluminium Surface Science and Technology*, H. Terryn and G. Verhoeven, Editors, p. 266 "Elzenveld," Antwerp, Belgium (1997).
43. P. Cabot, F. Centellas, E. Perez, and Virgili, *Electrochim. Acta*, **30**, 1035 (1985).
44. J. Dickey, J. Davidson, and Y. Tzeng, *J. Electrochem. Soc.*, **136**, 1772 (1989).
45. J. De Laet, H. Terryn, and J. Vereecken, *Electrochim. Acta*, **41**, 1155 (1996).
46. P. G. Sheasby, in *International Symposium on Aluminium Surface Science and Technology*, H. Terryn and G. G. Verhoeven, Editors, p. 170, "Elzenveld," Antwerp, Belgium (1997).
47. V. Parkhutik, V. Belov, and M. Chernyckh, *Electrochim. Acta*, **35**, 961 (1990).
48. R. De Levie, *Electrochim. Acta*, **8**, 751 (1963).
49. R. De Levie, *Electrochim. Acta*, **9**, 1231 (1964).
50. H.-K. Song, Y.-H. Jung, K.-H. Lee, and L. Dao, *Electrochim. Acta*, **44**, 3513 (1999).
51. D. Griffiths, *Introduction to Electrodynamics*, Prentice Hall, New York (1999).
52. J. Fleig and J. Maier, *Electrochim. Acta*, **41**, 1003 (1996).
53. E. Patrito, R. Torresi, E. Leiva, and V. Macagno, *J. Electrochem. Soc.*, **137**, 524 (1990).
54. *CRC Handbook of Chemistry and Physics*, 55th ed., R. Weast, Editor, CRC Press, Boca Raton, FL (1974/1975).
55. T. Libsch and O. Devereux, *J. Electrochem. Soc.*, **123**, 864 (1976).